Inorganic Chemistry

Article

pubs.acs.org/IC

# Spin−Orbit TDDFT Electronic Structure of Diplatinum(II,II) Complexes

Stanislav Záliš,*[,†] Yan-Choi Lam,[‡] Harry B. Gray,*[,‡] and Antonín Vlček*[,†,§]

[†]J. Heyrovský Institute of Physical Chemistry, Academy of Sciences of the Czech Republic, Dolejškova 3, CZ-182 23 Prague, Czech Republic

[‡]Beckman Institute, California Institute of Technology, Pasadena, California 91125, United States

[§]School of Biological and Chemical Sciences, Queen Mary University of London, Mile End Road, London E1 4NS, United Kingdom

Supporting Information

**ABSTRACT:** $[Pt_2(\mu\text{-}P_2O_5H_2)_4]^{4-}$ (Pt(pop)) and its perfluoroborated derivative $[Pt_2(\mu\text{-}P_2O_5(BF_2)_2)_4]^{4-}$ (Pt(pop-$BF_2$)) are $d^8$−$d^8$ complexes whose electronic excited states can drive reductions and oxidations of relatively inert substrates. We performed spin−orbit (SO) TDDFT calculations on these complexes that account for their absorption spectra across the entire UV−vis spectral region. The complexes exhibit both fluorescence and phosphorescence attributable, respectively, to singlet and triplet excited states of $d\sigma^*p\sigma$ origin. These features are energetically isolated from each other (~7000 $cm^{-1}$ for (Pt(pop-$BF_2$)) as well as from higher-lying states (5800 $cm^{-1}$). The lowest $^3d\sigma^*p\sigma$ state is split into three SO states by interactions with higher-lying singlet states with $d\pi p\sigma$ and, to a lesser extent, $p\pi p\sigma$ contributions. The spectroscopically allowed $d\sigma^*p\sigma$ SO state has ~96% singlet character with small admixtures of higher triplets of partial $d\pi p\sigma$ and $p\pi p\sigma$ characters that also mix with $^3d\sigma^*p\sigma$, resulting in a second-order $^1d\sigma^*p\sigma$−$^3d\sigma^*p\sigma$ SO interaction that facilitates intersystem crossing (ISC). All SO interactions involving the $d\sigma^*p\sigma$ states are weak because of large energy gaps to higher interacting states. The spectroscopically allowed $d\sigma^*p\sigma$ SO state is followed by a dense manifold of ligand-to-metal−metal charge transfer states, some with $p\pi p\sigma$ (at lower energies) or $d\pi p\sigma$ contributions (at higher energies). Spectroscopically active higher states are strongly spin-mixed. The electronic structure, state ordering, and relative energies are minimally perturbed when the calculation is performed at the optimized geometries of the $^1d\sigma^*p\sigma$ and $^3d\sigma^*p\sigma$ excited states (rather than the ground state). Results obtained for Pt(pop) are very similar, showing slightly smaller energy gaps and, possibly, an additional $^1d\sigma^*p\sigma$ − $^3d\sigma^*p\sigma$ second order SO interaction involving higher $^1d\pi p\sigma^*$ states that could account in part for the much faster ISC. It also appears that $^1d\sigma^*p\sigma \rightarrow {}^3d\sigma^*p\sigma$ ISC requires a structural distortion that has a lower barrier for Pt(pop) than for the more rigid Pt(pop-$BF_2$).

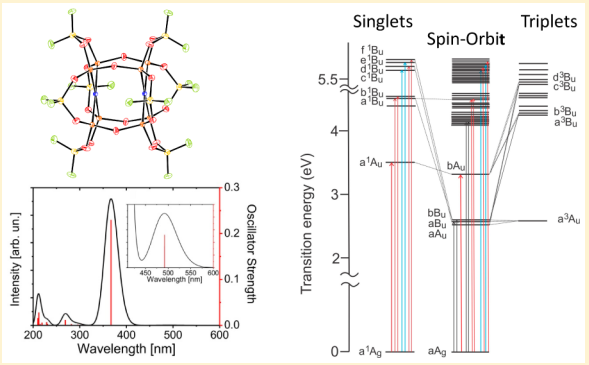


## INTRODUCTION

The singlet and triplet $d\sigma^* \rightarrow p\sigma$ excited states of dinuclear complexes of $d^8$ metals (Pt(II), Rh(I), Ir(I)) show remarkable photoactivity: strong emission, photoinduced electron and energy transfer as well as photochemical atom abstraction.[1−13] This behavior is well-represented by $[Pt_2(P_2O_5H_2)_4]^{4-}$ (further abbreviated Pt(pop)), whose electronic absorption spectrum features a very strong $^1(5d\sigma^* \rightarrow 6p\sigma)$ near-UV band accompanied by a much weaker absorption attributable to spin-forbidden $^3(5d\sigma^* \rightarrow 6p\sigma)$ transition at lower energy. In addition, more relatively weak absorption bands occur in the UV region.[5−7] The fluorescence is very weak and short-lived (~3 ps),[7,14] whereas phosphorescence occurs[7] with a 0.5−0.6 quantum yield and almost 10 $\mu$s lifetime in fluid solution. Recently, a perfluoroborated derivative $[Pt_2(P_2O_5(BF_2)_2)_4]^{4-}$ (Pt(pop-$BF_2$), Figure 1) was reported, where the pop ligands are covalently linked by rigid $BF_2$ groups instead of H-bonds.[1] Pt(pop) and Pt(pop-$BF_2$) have similar UV−vis absorption spectra but very different photophysics: notably, Pt(pop-$BF_2$) exhibits strong $^1d\sigma^*p\sigma \rightarrow {}^1(d\sigma^*)^2$ fluorescence whose 1.6 ns lifetime indicates that $^1d\sigma^*p\sigma \rightarrow {}^3d\sigma^*p\sigma$ intersystem crossing is $1 \times 10^3$ to $1 \times 10^4$ times slower than in the case of Pt(pop).[1] Interestingly, phosphorescence from the $^3d\sigma^*p\sigma$ state is comparable for both complexes. Temperature-dependent phosphorescence decay kinetics of Pt(pop) revealed[5,6,15] relatively large (41 $cm^{-1}$) zero-field splitting (zfs) of the $^3d\sigma^*p\sigma$ state ($^3A_{2u}$ in the $D_{4h}$ symmetry of the $Pt_2P_8$ core) into higher $E_u$ and lower $A_{1u}$ spin−orbit (SO) states; a comparable zfs value was determined[16] for Pt(pop-$BF_2$). Direct SO coupling between the singlet and triplet $A_{2u}$ ($d\sigma^*p\sigma$) states is forbidden within $D_{4h}$ core symmetry. A theoretical analysis by Azumi,[17] based on solving SO secular determinants between states arising from a limited set of four 5d and one 6p Pt atomic orbitals, attributed the occurrence of spin-forbidden absorption and phosphorescence to small admixtures of higher $^3E_u$ and $^1E_u$ states of $5d\pi \rightarrow 6p\sigma$ origin to the singlet and triplet $A_{2u}(d\sigma^*p\sigma)$ states, respectively.

**Received:** January 9, 2015
**Published:** March 16, 2015





DOI: 10.1021/acs.inorgchem.5b00063
*Inorg. Chem.* 2015, 54, 3491−3500

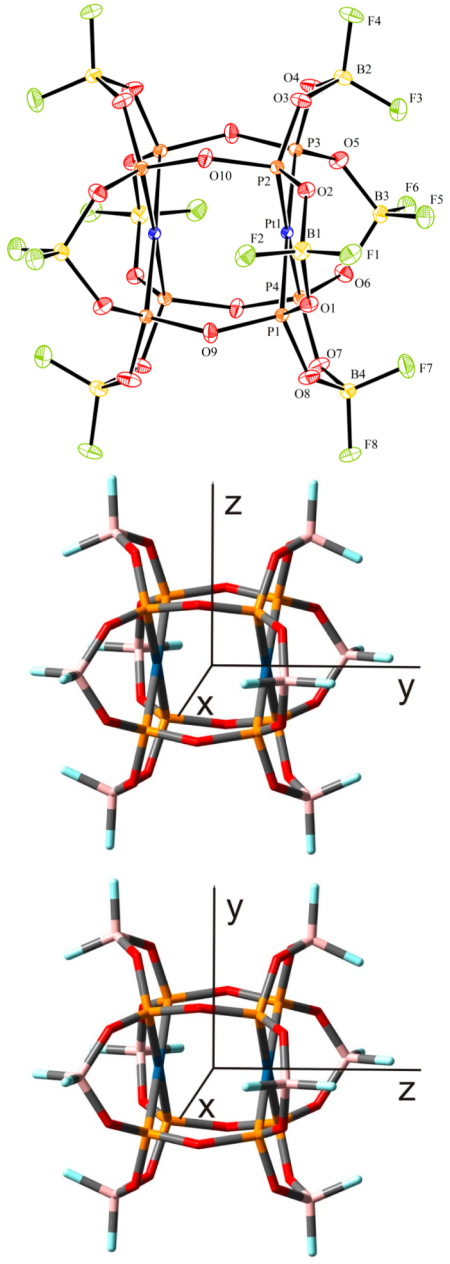


**Figure 1.** (upper) X-ray structure of Pt(pop-$BF_2$), CCDC 1049647. (center) DFT-optimized structure that corresponds to the experimental structure. The molecule has a $C_{2h}$ symmetry with the $C_2(z)$ axis oriented perpendicularly to the Pt–Pt axis. The $y$ and Pt–Pt axes are not collinear, containing an angle of 7.7°. (lower) Idealized $C_{2h}$ geometry with the $C_2(z)$ axis coinciding with Pt–Pt. Whereas the calculations were performed on the optimized geometry, the states and orbitals are labeled according to the idealized one.

Previous density functional theory (DFT) and time-dependent DFT (TDDFT) theoretical studies of Pt(pop) in vacuum revealed the occurrence of energetically close staggered and eclipsed conformations,[18] characterized IR and Raman active vibrations,[18] calculated structural changes on going to the $^3$d$\sigma^*$p$\sigma$ state[19,20] and analyzed Pt–Pt bonding in the ground and lowest triplet states.[19] Calculations performed in water (described by dielectric continuum models) pointed to the importance of including solvent,[20] reproduced reasonably well the spin-allowed $^1$d$\sigma^* \rightarrow$ p$\sigma$ transition,[20,21] and revealed partial O,P $\rightarrow$ Pt charge-transfer character of the next higher-lying UV transition, whereas no information is available on the nature of higher transitions in the UV. All these studies indicate that the singlet and triplet d$\sigma^*$p$\sigma$ states are relatively isolated, with no close-lying electronic state that could mediate intersystem crossing.

The occurrence of spin-forbidden bands in absorption and emission spectra of Pt(pop) and Pt(pop-$BF_2$) and the structure-dependent intersystem crossing rate call for a theoretical investigation of electronic states and transitions that explicitly includes SO coupling. With the goal of understanding the electronic spectra and SO coupling pathways, we performed perturbational SO TDDFT calculations (SO-TDDFT).[22−25] This approach has allowed us to formulate the electronic structures of these $d^8$–$d^8$ dinuclear complexes in terms of d$\sigma^*$p$\sigma$ SO states followed in energy by a block of relatively weak transitions to highly spin-mixed ligand-to-metal–metal charge transfer (LMMCT) states, with further Pt–Pt (5d, 6p)-based states at still higher energies. Nevertheless, it is these high-lying states that SO-couple with the lowest d$\sigma^*$p$\sigma$ singlet and triplet, enabling spin-forbidden absorption, zfs, and phosphorescence of the lowest triplet, as well as unusually slow and structure-sensitive intersystem crossing.

## COMPUTATIONAL DETAILS

The electronic structures of the Pt(pop-$BF_2$) and Pt(pop) complexes were calculated by DFT and TDDFT methods using the ADF2013.01[26,27] program package. Single-point TDDFT calculations were performed at DFT-optimized geometries. Structures of the lowest spin-free singlet and triplet excited states were optimized by unrestricted Kohn–Sham (UKS) approach.

Slater-type orbital (STO) basis sets of triple-$\zeta$ quality with two polarization functions for the Pt atom, triple-$\zeta$ with polarization functions for O, P, and H atoms, and double-$\zeta$ with one polarization function for the remaining atoms were employed. The basis set was represented by a frozen core approximation (1s for B, N, O, 1s-2p for P and 1s-4d for Pt were kept frozen). The calculations were performed with the Perdew, Burke, and Ernzerhof (PBE0) exchange and correlation functional.[28,29] The scalar relativistic (SR) zero-order regular approximation (ZORA) was used. Solvent-effect corrections were calculated using the COSMO model.[30]

In the first step, scalar relativistic TDDFT calculations were performed to determine low-lying spin-free excited states. In the second step, SO coupling was applied as a perturbation to obtain transition energies to SO excited states.[22−24] Lowest 20 spin-free states up to 6.3 eV and corresponding SO states were calculated. For comparison, several lowest-lying excited states also were calculated by the relativistic two-component zeroth-order regular approximation in the TDDFT method[22,23] with comparable results.

## SYNTHESIS AND CRYSTALLOGRAPHIC DETAILS

$[Ph_4As]_4[Pt_2(\mu\text{-}P_2O_5(BF_2)_2)_4]$ was prepared by stirring $[Ph_4As]_4[Pt_2(\mu\text{-}P_2O_5H_2)_4]$[31] in neat $F_3B{\cdot}OEt_2$ for 30 min at 50 °C, then at room temperature for 2 days. The product was isolated and purified as described[1] for $[n\text{-}Bu_4N]_4[Pt_2(\mu\text{-}P_2O_5(BF_2)_2)_4]$. Crystals suitable for single crystal diffraction were prepared by vapor diffusion of diethyl ether into MeCN solution, mounted on a glass fiber using Paratone oil, and placed on a Bruker Kappa Apex II diffractometer under a nitrogen stream. Structures were solved using the SHELX software and refined. The structure was deposited at the Cambridge Crystallographic Data Centre under the deposition No. CCDC 1049647. Full details of the crystal structure are available in the Supporting Information—"Crystal and Structural Data".



DOI: 10.1021/acs.inorgchem.5b00063
*Inorg. Chem.* 2015, 54, 3491−3500

## RESULTS

**Molecular Structure.** Ground-state molecular structures of Pt(pop-$BF_2$) and Pt(pop) optimized by DFT in vacuo closely match those determined experimentally. Selected experimental and calculated bonding parameters of Pt(pop-$BF_2$) are listed Table 1. Supporting Information, Table S1 compares Pt(pop-$BF_2$) and Pt(pop). The small Pt−Pt bond shortening on going from Pt(pop) to Pt(pop-$BF_2$) is confirmed by calculations. Geometries of Pt(pop-$BF_2$) and Pt(pop) calculated in MeCN with a COSMO solvent correction are summarized in Table 2, together with those of the lowest triplet and singlet excited states. Pt−Pt bond shortening is the only significant structural effect of excitation. The lowest singlet and triplet excited states of Pt(pop-$BF_2$) have almost identical structures, the Pt−Pt bond being shortened by ∼0.18 Å relative to the ground state because of[2,3,5−7,10] depopulation of a $\sigma$-antibonding and population of a bonding orbital upon $d\sigma^* \rightarrow p\sigma$ excitation. For Pt(pop), the Pt−Pt bond in the excited triplet was calculated ∼0.02 Å shorter than in the excited singlet (Table 2).

**Table 1. Selected Bond Lengths (Å) and Angles (deg) of Pt(pop-$BF_2$) Calculated by DFT/PBE0 in Vacuo and Crystallographically Determined Values for $[Ph_4As]_4[Pt_2(pop\text{-}BF_2)_4]$**

| bond | exp | calc |
|---|---|---|
| Pt1−Pt1′ | 2.8873(11) | 2.918 |
| Pt1−P1 | 2.2872(3) | 2.313 |
| Pt1−P2 | 2.2938(3) | 2.313 |
| Pt1−P3 | 2.2943(3) | 2.313 |
| Pt1−P4 | 2.2960(3) | 2.313 |
| P1−O1 | 1.5411(9) | 1.565 |
| P1−O8 | 1.5390(9) | 1.563 |
| P1−O9 | 1.6174(9) | 1.646 |
| O1−B1 | 1.4946(16) | 1.494 |
| O2−B1 | 1.4777(15) | 1.494 |
| B1−F1 | 1.3802(15) | 1.402 |
| B1−F2 | 1.3790(15) | 1.402 |
| angle | | |
| Pt1′−Pt1−P2 | 91.993(7) | 91.4 |
| Pt1−P1−O1 | 115.71(3) | 116.4 |
| Pt1−P1−O8 | 117.23(4) | 116.4 |
| Pt1−P1−O9 | 110.82(3) | 110.9 |
| P1−Pt1−P2 | 88.756(10) | 88.17 |
| P1−Pt1−P4 | 91.304(10) | 91.85 |
| P1−Pt1−P3 | 178.272(10) | 177.7 |
| P1−O9−P1′ | 132.56(5) | 132.15 |

Pt(pop-$BF_2$) in $[Ph_4As]_4[Pt(pop\text{-}BF_2)]$ crystals has $C_{2h}$ symmetry with the $C_2(z)$ axis oriented perpendicular to the Pt−Pt axis that deviates by 7.7° with respect to the $y$-axis of the coordinate system (Figure 1, upper). This structure, as reproduced by DFT optimization (Figure 1, center), was used for all electronic structure calculations reported below. However, to ensure compatibility with the results on Pt(pop) and previous literature on $d^8$−$d^8$ systems, the states and orbitals are labeled according to an idealized structure with coincident $C_2(z)$ and Pt−Pt axes (Figure 1, lower). In addition, symmetry labels corresponding to idealized $D_{4h}$ $Pt_2P_8$ core symmetry are stated in parentheses.

Pt(pop) occurs in two stable conformations,[18] namely, staggered and eclipsed (Supporting Information, Figure S1). Electronic structure calculations reported below were performed on the more stable (by 0.012 eV) $C_{4h}$ eclipsed conformation. For compatibility with the Pt(pop-$BF_2$) calculation, we used $C_{2h}$ symmetry labeling with coincident $C_2(z)$ and Pt−Pt axes.

**Table 2. Selected Bond Lengths (Å) of Pt(pop-$BF_2$) and Pt(pop) in the Electronic Ground State ($a^1A_g$), Lowest Excited Triplet ($a^3A_u$), and Lowest Excited Singlet ($b^1A_u$) States Calculated by DFT(COSMO-MeCN)**

| bond | calculated | | | | | |
|---|---|---|---|---|---|---|
| Pt(pop-$BF_2$) | $a^1A_g$ (GS) | $a^3A_u$ | $\Delta(a^3A_u$-GS) | $b^1A_u$ | $\Delta(b^1A_u$-GS) | $\Delta(b^1A_u$-$a^3A_u$) |
| Pt−Pt | 2.904 | 2.725 | −0.179 | 2.724 | −0.180 | −0.001 |
| Pt−P (average) | 2.308 | 2.312 | 0.004 | 2.318 | 0.010 | 0.006 |
| P−O(-P) (average) | 1.641 | 1.638 | −0.003 | 1.645 | 0.004 | 0.007 |
| Pt(pop) eclipsed | | | | | | |
| Pt−Pt | 2.924 | 2.742 | −0.182 | 2.745 | −0.156 | 0.003 |
| Pt−P (average) | 2.332 | 2.337 | 0.005 | 2.337 | 0.002 | 0.000 |
| P−O(-P) (average) | 1.660 | 1.658 | −0.002 | 1.661 | 0.000 | 0.003 |
| Pt(pop) staggered | | | | | | |
| Pt−Pt | 2.901 | 2.731 | −0.170 | 2.745 | −0.156 | 0.014 |
| Pt−P (average) | 2.334 | 2.336 | 0.002 | 2.337 | 0.002 | 0.001 |
| P−O(-P) (average) | 1.661 | 1.660 | −0.001 | 1.661 | 0.000 | 0.001 |

To check for possible structural effects of the solvent and counter-cations, a cluster containing Pt(pop) anion, four $Me_4N^+$, and two MeCN molecules, all imbedded in MeCN solvent modeled by COSMO, was calculated by DFT. The resulting structure (Supporting Information, Figure S2) shows the four cations arranged around Pt(pop) approximately in the $\sigma_h$ plane and the MeCN molecules oriented perpendicularly to the Pt−Pt axis, one on each side of the complex ion (3.7 Å apart). The molecular and electronic structures of Pt(pop) in the cluster are very similar to those calculated for isolated Pt(pop) in MeCN solution.

**Electronic Structure of Pt(pop-$BF_2$): Molecular Orbitals.** The compositions of spin-free DFT-calculated frontier molecular orbitals of Pt(pop-$BF_2$) are listed in Supporting Information, Table S2, and the spectroscopically relevant MOs are depicted in Figure 2. In accord with the generally accepted bonding model of $d^8$−$d^8$ complexes, the highest occupied molecular orbital (HOMO) and lowest unoccupied molecular orbital (LUMO) have major contributions from Pt−Pt $5d\sigma^*$ and $6p\sigma$ orbitals, respectively. The HOMO has 83% Pt character, whereas the LUMO is 44% Pt and delocalized over the pop-$BF_2$ ligand framework (56%). Importantly, the HOMO−LUMO set is energetically separated from the rest of the MOs. The energy gaps between HOMO and HOMO−1 (1.17 eV) and between LUMO and LUMO+1 (2.32 eV) are large relative to those between lower occupied MOs (spaced by tenths of electronvolts). The levels HOMO−1 to HOMO−4 are mainly formed by combinations of ligand p orbitals with small Pt-6p contributions (8−12%). Lower-lying $46,45b_u$ levels are primarily oxygen-localized orbitals with small fluorine contributions. Levels $44,43b_u$ are Pt−Pt $d\pi$ orbitals (66%) extending over the bridging O atoms and terminal $BF_2$ groups. LUMO+1 ($44a_u$) and LUMO+2 ($49a_g$) are Pt−P $\sigma^*$ orbitals ($\sigma$



DOI: 10.1021/acs.inorgchem.5b00063
Inorg. Chem. 2015, 54, 3491−3500

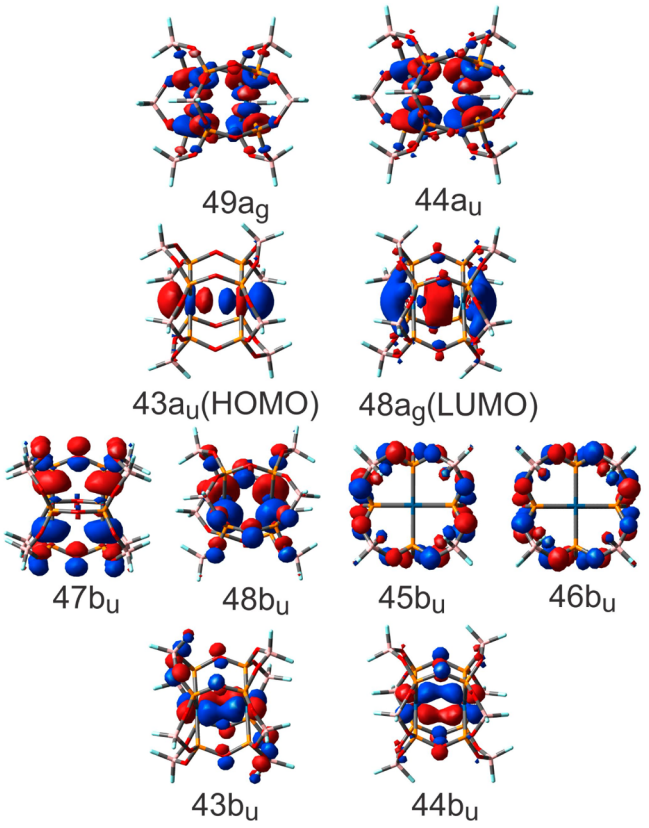


**Figure 2.** DFT (COSMO-MeCN) spectroscopically relevant molecular orbitals of Pt(pop-$BF_2$) viewed perpendicularly to the Pt−Pt axis (except for $45b_u$ and $46b_u$, viewed in the Pt−Pt direction.).

ligand orbitals with ∼30% Pt $d_{xy}\delta/\delta^*$ contributions). The energy ordering and characters of Pt(pop) frontier MOs (Supporting Information, Table S3) are very similar to those of Pt(pop-$BF_2$).

**Spin−Orbit Electronic States of Pt(pop-$BF_2$).** Results from calculations of spin-free (i.e., singlet and triplet) excited states of Pt(pop-$BF_2$) and Pt(pop) are summarized in Table 3 and Supporting Information, Table S4, respectively. Spectroscopically relevant transitions are nearly pure (≥94%) single one-electron excitations to the 6p$\sigma$ LUMO. Higher excitations originating in predominantly pop-$BF_2$ ligand orbitals transfer electron density from the ligands to the Pt−Pt bond (labeled LMMCT, ligand to metal−metal charge transfer).

Calculated SO transitions of both complexes account well for all the features observed in the experimental absorption spectra (Figure 3). The predicted maximum (367 nm) of the strongly allowed $aA_g \rightarrow bA_u$ ($d\sigma^* \rightarrow p\sigma$) transition matches the experimental value of 365 nm,[1] whereas the corresponding $aA_g \rightarrow a,bB_u$ spin-forbidden band was calculated to fall at somewhat longer wavelength (493 nm) than observed (454 nm). The relative intensity of the spin-forbidden absorption band was underestimated by the SO calculations: predicted 535 oscillator-strength ratio of the $aA_g \rightarrow bA_u$ and $aA_g \rightarrow a,bB_u$ transitions is greater than observed band area ratio (136). The poor agreement could be caused by neglecting spin-vibronic contributions to $aA_g \rightarrow a,bB_u$ intensities. Nevertheless, SO-TDDFT correctly indicates higher intensity of the spin-forbidden $aA_g \rightarrow a,bB_u$ transition in Pt(pop-$BF_2$) as compared with Pt(pop) (Figure 3).

**Table 3. Spectroscopically and Photophysically Relevant Spin-Free Electronic Transitions of Pt(pop-$BF_2$)**

| state | main components (%) | calculated transitions[a] | oscillator strength |
|---|---|---|---|
| $a^3A_u$ ($a^3A_{2u}$), Pt(d$\sigma^*$) → Pt(p$\sigma$) | 99 ($43a_u \rightarrow 48a_g$) | 2.58 (480) | |
| $a^1A_u$($a^1A_{2u}$), Pt(d$\sigma^*$) → Pt(p$\sigma$) | 98 ($43a_u \rightarrow 48a_g$) | 3.46 (358) | 0.241 |
| $a^3B_u$($a^3E_u$), LMMCT/Pt(p$\pi$) → Pt(p$\sigma$) | 97 ($48b_u \rightarrow 48a_g$) | 4.19 (296) | |
| $b^3B_u$($a^3E_u$), LMMCT/Pt(p$\pi$) → Pt(p$\sigma$) | 95 ($47b_u \rightarrow 48a_g$) | 4.24 (292) | |
| $a^3B_g$($a^3E_g$), LMMCT | 97 ($44b_g \rightarrow 48a_g$) | 4.25 (291) | |
| $a^1B_g$($a^1E_g$), LMMCT | 97 ($44b_g \rightarrow 48a_g$) | 4.39 (282) | 0.000 |
| $b^3B_g$($a^3E_g$), LMMCT | 95 ($43b_g \rightarrow 48a_g$) | 4.43 (279) | |
| $a^1B_u$($a^1E_u$), LMMCT/Pt(p$\pi$) → Pt(p$\sigma$) | 99 ($48b_u \rightarrow 48a_g$) | 4.55 (272) | 0.010 |
| $b^1B_u$($a^1E_u$), LMMCT/Pt(p$\pi$) → Pt(p$\sigma$) | 99 ($47b_u \rightarrow 48a_g$) | 4.55 (272) | 0.013 |
| $b^1A_g$($a^1A_{1g}$) LMMCT | 98 ($47b_g \rightarrow 48a_g$) | 4.63 (268) | 0.000 |
| $c^3B_g$($b^3E_g$), Pt(d$\pi^*$) → Pt(p$\sigma$) | 99 ($42b_g \rightarrow 48a_g$) | 4.77 (260) | |
| $d^3B_g$($b^3E_g$), Pt(d$\pi^*$) → Pt(p$\sigma$) | 99 ($43b_g \rightarrow 48a_g$) | 4.80 (258) | |
| $b^3A_g$($a^3A_{1g}$), Pt(d$\sigma^*$) → Pt(d$\delta^*$)/$\sigma^*$(PtP) | 98 ($43a_u \rightarrow 44a_u$) | 4.84 (256) | |
| $d^3A_u$($b^3A_{2u}$), Pt(d$\sigma^*$) → Pt(d$\delta$)/$\sigma^*$(PtP) | 98 ($43a_u \rightarrow 49a_g$) | 4.86 (255) | |
| $c^1B_g$($c^1E_g$), Pt(d$\pi^*$) → Pt(p$\sigma$) | 99 ($42b_g \rightarrow 48a_g$) | 5.08 (244) | 0.000 |
| $d^1B_g$($c^1E_g$), Pt(d$\pi^*$) → Pt(p$\sigma$) | 99 ($43b_g \rightarrow 48a_g$) | 5.09 (244) | 0.000 |
| $b^1A_g$($a^1A_{1g}$), Pt(d$\sigma^*$) → Pt(d$\delta^*$)/$\sigma^*$(PtP) | 98 ($43a_u \rightarrow 44a_u$) | 5.12 (242) | 0.000 |
| $d^1A_u$($b^1A_{2u}$), Pt(d$\sigma^*$) → Pt(d$\delta$)/$\sigma^*$(PtP) | 98 ($43a_u \rightarrow 49a_g$) | 5.21 (238) | 0.000 |
| $c^3B_u$($c^3E_u$), Pt(d$\pi$) → Pt(p$\sigma$) | 84 ($43b_u \rightarrow 48a_g$) | 5.40 (230) | |
| $d^3B_u$($c^3E_u$), Pt(d$\pi$) → Pt(p$\sigma$) | 81 ($44b_u \rightarrow 48a_g$) | 5.41 (229) | |
| $c^1B_u$($d^1E_u$), LMMCT | 99 ($46b_u \rightarrow 48a_g$) | 5.66 (219) | 0.005 |
| $d^1B_u$($e^1E_u$), Pt(d$\pi$) → Pt(p$\sigma$) | 94 ($43b_u \rightarrow 48a_g$) | 5.75 (216) | 0.036 |
| $e^1B_u$($d^1E_u$), LMMCT | 98 ($45b_u \rightarrow 48a_g$) | 5.77 (215) | 0.003 |
| $f^1B_u$($e^1E_u$), Pt(d$\pi$) → Pt(p$\sigma$) | 95 ($44b_u \rightarrow 48a_g$) | 5.83 (213) | 0.027 |

[a]Transition energies in eV, with the corresponding wavelengths (nm) in parentheses. Symmetry labeling corresponds to idealized $C_{2h}$ symmetry. ($D_{4h}$ labels in parentheses.) TDDFT (COSMO-MeCN) calculation.

UV spectra below 365 nm for both complexes feature a series of relatively weak bands attributable to a large number of electronic transitions. This behavior cannot be accounted for by spin-free calculations (Table 3 and Supporting Information, Table S4) that predict only one LMMCT band (272 nm) and a stronger absorption below 220 nm for Pt(pop-$BF_2$). On the other hand, SO calculations produce a series of moderately intense mixed-spin transitions of LMMCT origin that correspond well to the observed absorptions (Tables 4 and 5, Figure 3). Somewhat stronger transitions to d$\pi^*$p$\sigma$ states with significant Pt(5d) contributions occur at higher energies (above


DOI: 10.1021/acs.inorgchem.5b00063
Inorg. Chem. 2015, 54, 3491−3500

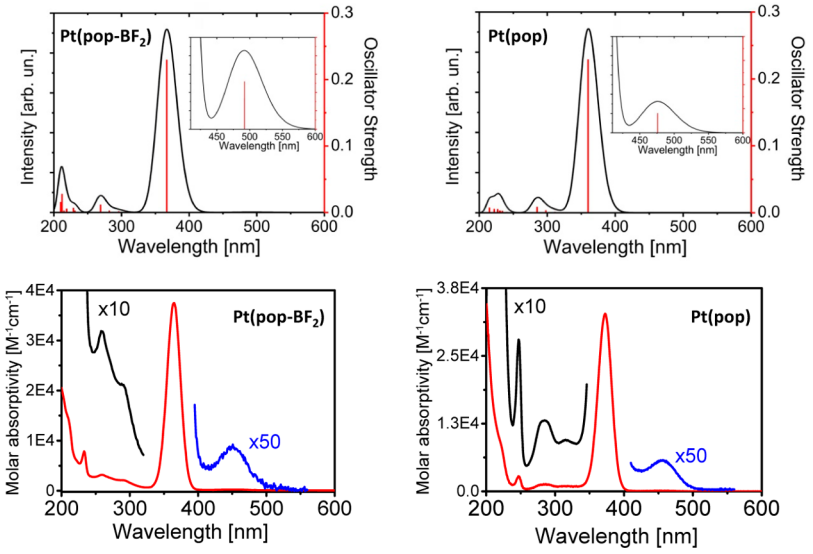


**Figure 3.** (upper) SO-TDDFT/COSMO-MeCN calculated UV−vis spectra of Pt(pop-$BF_2$) (left) and Pt(pop) (right). (insets) The lowest spin-forbidden transitions. (lower) Corresponding experimental spectra in MeCN. (Gaussian band shapes with fwhm of 2500 $cm^{-1}$ were used to simulate the spectra.).

**Table 4. Spectroscopically and Photophysically Relevant Spin−Orbit Electronic Transitions of Pt(pop-$BF_2$)**

| SO state | contributions of spin−free states | character | energy ($cm^{-1}$) | $\Delta E^a$ ($cm^{-1}$) | $\lambda$ (nm) | oscillator strength | exptl (nm) |
|---|---|---|---|---|---|---|---|
| $aA_u$ ($aA_{1u}$) | $a^3A_u$ (98%) + $c^3B_u$ (0.8%) + $d^3B_u$ (0.9%) + $b^3B_u$ (0.3%) | d$\sigma$*→p$\sigma$ | 20 278 | 0 | 493 | 0 | |
| $aB_u$ ($aE_u$) | $a^3A_u$ (98%) + $d^1B_u$ (0.7%) + $c^3B_u$ (0.9%) + $b^3B_u$ (0.3%) | d$\sigma$*→p$\sigma$ | 20 332 | 54 | 493 | 0.000 26 | 453 |
| $bB_u$ ($aE_u$) | $a^3A_u$ (98%) + $f^1B_u$ (0.5%) + $a^1B_u$ (0.2%) + $b^3B_u$ (0.9%) | d$\sigma$*→p$\sigma$ | 20 338 | 60 | 492 | 0.000 17 | |
| $bA_u$ ($aA_{2u}$) | $a^1A_u$ (95.6%) + $c^3B_u$ (1.4%) + $d^3B_u$ (1.4%) + $a^3B_u$ (0.9%) + $b^3B_u$ (0.6%) | d$\sigma$*→p$\sigma$ | 27 244 | 6966 | 367 | 0.230 | 364 |
| $cA_u$ ($bE_u$) | $a^3B_u$ (50%) + $b^3B_u$ (50%) | LMMCT p$\pi$→p$\sigma$ | 33 076 | 12 798 | 302 | 0.000 | |
| $dA_u$ ($bE_u$) | $a^3B_u$ (50%) + $b^3B_u$ (50%) | LMMCT p$\pi$→p$\sigma$ | 33 076 | 12 798 | 302 | 0.000 | |
| $aA_g$ ($cE_u$) | $a^3B_g$ (50%) + $b^3B_g$ (50%) | LMMCT | 33 304 | 13 026 | 300 | 0.000 | |
| $bA_g$ ($cE_u$) | $a^3B_g$ (50%) + $b^3B_g$ (50%) | LMMCT | 33 314 | 13 036 | 300 | 0.000 | |
| $cB_u$ ($dE_u$) | $a^3B_u$ (89%) + $b^1B_u$ (11%) | LMMCT p$\pi$→p$\sigma$ | 33 788 | 13 510 | 296 | 0.002 | |
| $dB_u$ ($dE_u$) | $b^3B_u$ (89%) + $a^1B_u$ (11%) | LMMCT p$\pi$→p$\sigma$ | 33 855 | 13 577 | 295 | 0.001 | |
| $eA_u$ ($bA_{2u}$) | $b^3B_u$ (51%) + $b^3B_u$ (49%) + $a^1A_u$ (2%) | LMMCT p$\pi$→p$\sigma$ | 35 468 | 15 190 | 282 | 0.003 | |
| $cA_g$ ($E_g$) | $c^3B_g$(40%) + $d^3B_g$(52%) + $c^1A_g$(3%) | d$\pi$*→p$\sigma$ LMMCT | 36 746 | 16 468 | 272 | 0.000 | |
| $dA_g$ ($E_g$) | $b^3A_g$ (24%) + $d^3B_g$(60%) + $c^1A_g$(10%) | d$\pi$*→p$\sigma$ LMMCT | 36 812 | 16 534 | 272 | 0.000 | |
| $aB_g$ ($E_g$) | $c^3B_g$(41%) + $d^3B_g$(50%) | d$\pi$*→p$\sigma$ LMMCT | 36 945 | 16 667 | 272 | 0.000 | |
| $cB_u$ ($eE_u$) | $a^1B_u$ (86%) + $b^3B_u$ (13%) | LMMCT p$\pi$→p$\sigma$ | 37 184 | 16 906 | 269 | 0.012 | 259 |
| $dB_u$ ($eE_u$) | $b^1B_u$ (86%) + $a^3A_u$ (13%) | LMMCT | 37 194 | 16 916 | 269 | 0.009 | |
| $fA_u$ ($cA_{2u}$) | $a^3B_u$ (49%) + $b^3B_u$ (50%) + $a^1A_u$ (1%) | LMMCT p$\pi$→p$\sigma$ | 43 276 | 22 998 | 231 | 0.003 | 233 222sh 208sh |
| $eB_u$ ($fE_u$) | $d^3B_u$ (80%) + $d^1B_u$ (20%) | LMMCT | 43 561 | 23 283 | 229 | 0.007 | |
| $fB_u$ ($fE_u$) | $c^1B_u$ (98%) | LMMCT | 45 624 | 25 346 | 219 | 0.005 | |
| $gB_u$($gE_u$) | Mixed | LMMCT | 45 660 | 25 382 | 219 | 0.006 | |
| $hB_u$ ($hE_u$) | $d^1B_u$ (78%) + $c^3B_u$ (18%) + $a^1B_u$ (2%) | d$\pi$→p$\sigma$ LMMCT | 47 236 | 26 958 | 212 | 0.028 | |
| $iB_u$ ($gE_u$) | $e^1B_u$ (67%) + $e^1B_u$ (28%) | LMMCT | 47 587 | 27 309 | 210 | 0.007 | |
| $jB_u$ ($hE_u$) | $f^1B_u$ (58%) + $d^3B_u$ (33%) | LMMCT d$\pi$→p$\sigma$ | 47 677 | 27 399 | 210 | 0.016 | |

[a] $\Delta E$ is the energy difference from the lowest SO excited state. Symmetry labeling corresponds to idealized $C_{2h}$ symmetry. ($D_{4h}$ labels in parentheses.) Calculation: SO TDDFT (COSMO-MeCN).



DOI: 10.1021/acs.inorgchem.5b00063
*Inorg. Chem.* 2015, 54, 3491−3500

Table 5. Spectroscopically and Photophysically Relevant Spin−Orbit Electronic Transitions of Pt(pop)

| SO state | contributions of spin−free states | character | energy ($cm^{-1}$) | $\Delta E^a$ ($cm^{-1}$) | $\lambda$ (nm) | osc str | expt |
|---|---|---|---|---|---|---|---|
| $aA_u$ ($aA_{1u}$) | $a^3A_u$ (98%) + $c^3B_u$ (0.9%) + $d^3B_u$ (0.9%) + $a^3B_u$ (0.2%) | $d\sigma^*\rightarrow p\sigma$ | 20 528 | 0 | 487 | 0 | |
| $aB_u$ ($aE_u$) | $a^3A_u$ (98%) + $e^1B_u$ (0.4%) + $d^1B_u$ (0.2%) + $d^3B_u$ (0.7%) | $d\sigma^*\rightarrow p\sigma$ | 20 588 | 60 | 486 | 0.000 10 | 456 |
| $bB_u$ ($aE_u$) | $a^3A_u$ (98%) + $f^1B_u$ (0.4%) + $d^1B_u$ (0.2%) + $c^3B_u$ (0.9%) | $d\sigma^*\rightarrow p\sigma$ | 20 588 | 60 | 486 | 0.000 10 | |
| $bA_u$ ($aA_{2u}$) | $a^1A_u$ (95%) + $c^3B_u$ (1.5%) + $d^3B_u$ (1.5%) + $a^3B_u$ (0.8%) + $b^3B_u$ (0.8%) + $e^1B_u$ (0.2%) + $f^1B_u$ (0.1%) | $d\sigma^*\rightarrow p\sigma$ | 27 182 | 6654 | 368 | 0.238 | 372 |
| $cA_u$ ($bE_u$) | $a^3B_u$ (50%) + $b^3B_u$ (49%) | LMMCT $p\pi\rightarrow p\sigma$ | 31 379 | 10 851 | 319 | 0.000 | |
| $dA_u$ ($bE_u$) | $a^3B_u$ (50%) + $b^3B_u$ (49%) | LMMCT $p\pi\rightarrow p\sigma$ | 31 380 | 10 852 | 319 | 0.000 | |
| $aA_g$ ($aE_g$) | $a^3B_g$ (50%) + $b^3B_g$ (50%) | LMMCT | 31 427 | 10 899 | 318 | 0.000 | |
| $bA_g$ ($aE_g$) | $a^3B_g$ (50%) + $b^3B_g$ (50%) | LMMCT | 31 427 | 10 899 | 318 | 0.000 | |
| $aB_g$ ($bE_g$) | $a^3B_g$ (77%) + $b^1B_g$ (20%) | LMMCT | 31 898 | 11 370 | 313 | 0.000 | |
| $bB_g$ ($bE_g$) | $b^3B_g$ (73%) + $a^1B_g$ (20%) | LMMCT | 31 905 | 11 377 | 313 | 0.000 | |
| $cB_u$ ($cE_u$) | $a^3B_u$ (85%) + $b^1B_u$ (13%) | LMMCT $p\pi\rightarrow p\sigma$ | 32 030 | 11 502 | 312 | 0.001 | 315 |
| $dB_u$ ($cE_u$) | $b^3B_u$ (81%) + $a^1B_u$ (13%) | LMMCT $p\pi\rightarrow p\sigma$ | 32 044 | 11 516 | 312 | 0.001 | |
| $eA_u$ ($bA_{2u}$) | $a^3B_u$ (48%) + $b^3B_u$ (47%) + $a^1A_u$ (2%) | LMMCT $p\pi\rightarrow p\sigma$ | 33 498 | 12 970 | 298 | 0.003 | 284 |
| $eB_u$ ($dE_u$) | $a^1B_u$ (86%) + $b^3B_u$ (13%) | LMMCT $p\pi\rightarrow p\sigma$ | 34 995 | 14 467 | 286 | 0.009 | |
| $fB_u$ ($dE_u$) | $b^1B_u$ (86%) + $a^3A_u$ (13%) | LMMCT | 35 009 | 14 481 | 286 | 0.009 | |
| $gB_u$ ($eE_u$) | $d^3B_u$ (82%) + $c^1B_u$ (10%) | LMMCT | 41 172 | 20 644 | 243 | 0.002 | 247 |
| $hB_u$ ($eE_u$) | $c^3B_u$ (40%) + $d^3B_u$ (32%) + $a^1A_u$ (2%) | LMMCT | 41 177 | 20 649 | 243 | 0.002 | |
| $fA_u$ ($cA_{2u}$) | $c^3B_u$ (82%) + $d^1B_u$ (10%) | LMMCT | 42 581 | 22 053 | 235 | 0.004 | |
| $iB_u$ ($fE_u$) | $e^3B_u$ (78%) + $c^1B_u$ (18%) | LMMCT | 43 130 | 22 602 | 232 | 0.003 | |
| $jB_u$ ($fE_u$) | $e^3B_u$ (72%) + $c^1B_u$ (24%) | | 43 134 | 22 606 | 232 | 0.003 | |
| $kB_u$($gE_u$) | $c^1B_u$ (45%) + $e^1B_u$ (15%) | LMMCT | 43 968 | 23 440 | 227 | 0.007 | ≤220sh |
| $lB_u$ ($gE_u$) | $d^1B_u$ (45%) + $f^1B_u$ (15%) | LMMCT | 43 985 | 23 457 | 227 | 0.007 | |
| $gA_u$ ($dA_{2u}$) | $e^3B_u$ (42%) + $c^1B_u$ (33%) + $a^1A_u$ (2%) | mixed | 44 774 | 24 246 | 223 | 0.005 | |
| $mB_u$ ($hE_u$) | $e^1B_u$ (80%) + $f^3B_u$ (8%) | $d\pi\rightarrow p\sigma$ LMMCT | 46 100 | 25 572 | 217 | 0.008 | |
| $nB_u$ ($hE_u$) | $f^1B_u$ (80%) + $e^3B_u$ (8%) | $d\pi\rightarrow p\sigma$ LMMCT | 46 110 | 25 582 | 217 | 0.008 | |

[a] $\Delta E$ is the energy difference from the lowest SO excited state. Symmetry labeling corresponds to idealized $C_{2h}$ symmetry. ($D_{4h}$ labels in parentheses.) Calculation: SO TDDFT (COSMO-MeCN).

47 000 $cm^{-1}$): $hB_u$ and $jB_u$ likely contribute to the strong absorptions at the short-wavelength end of the UV spectrum. (The situation is very similar for Pt(pop), where all the UV bands are red-shifted relative to their Pt(pop-$BF_2$) counterparts. These shifts are well-reproduced by SO-TDDFT (compare Tables 4 and 5). In particular, the $d\pi^*p\sigma$ states m,n$B_u$ occur in Pt(pop) > 46 000 $cm^{-1}$. The calculated spectrum of the staggered form of Pt(pop) does not differ from that of the eclipsed conformation. The main intense absorption feature is calculated at 27 241 $cm^{-1}$; zfs is 66 $cm^{-1}$.)

The SO interaction gives rise to states that are expressed as linear combinations of contributing singlets and triplets (Table 4 and Figure 4; Table 5 for Pt(pop)). The $d\sigma^*p\sigma$ states retain singlet and triplet characters, to a large extent. The lowest triplet state $a^3A_u$ is split into three SO states (aAu, a,b$B_u$), owing to small admixtures of higher-lying $^1B_u$ states $d^1$,$f^1B_u$ and (to a lesser extent) $a^1B_u$ that contain contributions from $5d\pi$ and $6p\pi$ Pt orbitals perpendicular to the Pt−Pt axis, respectively.

The $a^3A_u$ zfs was calculated as 60 $cm^{-1}$, somewhat larger than the experimental value[16] of 40 $cm^{-1}$. The spectroscopically allowed $bA_u$ state is 95.6% $^1d\sigma^*p\sigma$, along with small contributions from higher $^3d\pi p\sigma$ d,$f^3B_u$ and $^3$LMMCT/$p\pi p\sigma$ a,$b^3B_u$ states. High-lying states are affected by SO coupling much more than the $d\sigma^*p\sigma$ states, with 10−30% singlet−triplet mixing. A dense manifold of LMMCT SO states is predicted at >5800 $cm^{-1}$ above $bA_u$ ($d\sigma^*p\sigma$) for Pt(pop-$BF_2$) [>4100 $cm^{-1}$ for Pt(pop)].

**Spin−Orbit States at Excited-State Geometries.** Excitation to singlet and triplet $aA_u$ ($d\sigma^*p\sigma$) states shortens the Pt−Pt bond by ∼0.18 Å (Table 2). To determine the effect of $d\sigma^* \rightarrow p\sigma$ excitation and ensuing Pt−Pt shortening on the excited-state manifold, we performed an SO-TDDFT calculation at the optimized geometries of the $a^1A_u$ and $a^3A_u$ spin-free states. Of interest is that the Pt−Pt contraction does not change the character and ordering of low-lying SO states; and, importantly, no electronic state emerges in the energetic proximity of the $bA_u$ state or between $bA_u$ and the $aA_u$/$bB_u$/$bB_u$ manifold, whose energy gap slightly increases (by 65 $cm^{-1}$), and the overall triplet admixture into $bA_u$ decreases from 4.3 to 3.1%. (Table 6, Figure 5). Upper states are also slightly stabilized; the energy gap between $bA_u$ and the next higher SO states decreases by 163 $cm^{-1}$. The SO-TDDFT calculation at the optimized $a^1A_u$ geometry of the Pt(pop) (Supporting Information, Table S5) shows similar trends. The calculated $bA_u$ energy of Pt(pop-$BF_2$) at the $a^1A_u$ geometry (25 252 $cm^{-1}$) closely matches the experimental fluorescence energy of 25 445 $cm^{-1}$, whereas that for a,$bB_u$ at the $a^3A_u$ geometry (18 216 $cm^{-1}$) underestimates the energy of phosphorescence (19 531 $cm^{-1}$).



DOI: 10.1021/acs.inorgchem.5b00063
Inorg. Chem. 2015, 54, 3491−3500

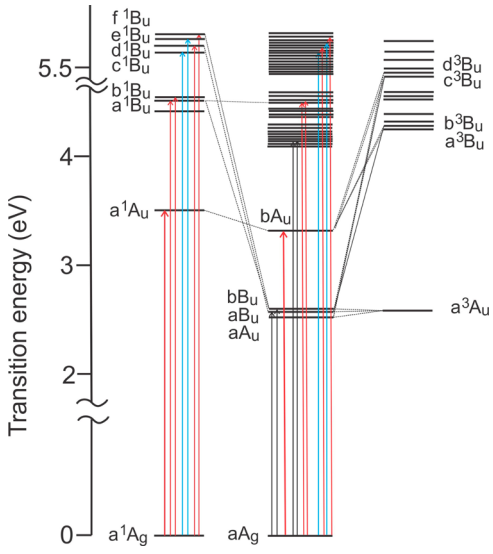


**Figure 4.** Correlation of calculated (TDDFT) lowest singlet (left) and triplet (right) spin-free states with SO states (middle) of Pt(pop-$BF_2$). Red, blue, and black arrows indicate transitions with oscillator strengths larger than 0.01, 0.001−0.01, and 0.0005−0.001, respectively. Symmetry labeling corresponds to idealized $C_{2h}$ symmetry. Calculation: SO-TDDFT (COSMO-MeCN).

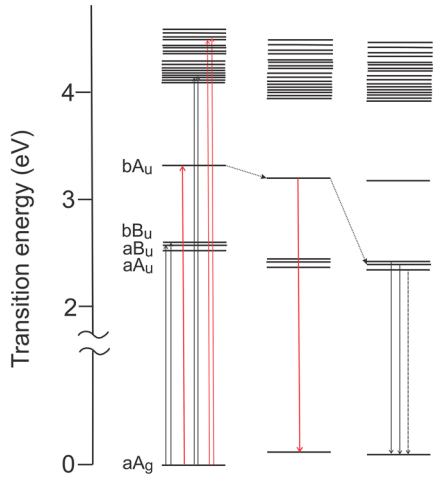


**Figure 5.** Correlation of SO TDDFT states of Pt(pop-$BF_2$) at the optimized ground state (left), lowest singlet ($a^1A_u$, center), and lowest triplet ($a^3A_u$ right) geometries. Red, blue, and black arrows indicate transitions with oscillator strengths larger than 0.01, 0.001−0.01, and 0.0005−0.001, respectively. The dotted arrows indicate the evolution of the optically excited $bA_u$ state (ISC).

## DISCUSSION

Pt(pop-$BF_2$) and Pt(pop) have very similar electronic structures. Their frontier MOs have analogous characters and orderings. A large energetic separation of 5d$\sigma$* HOMO and 6p$\sigma$ LUMO from lower occupied and higher unoccupied MOs, respectively, 53−56% delocalization of the 6p$\sigma$ LUMO over the ligand cluster, a block of ligand-localized (in some cases with ∼10% Pt 6p$\pi$) occupied MOs lying below HOMO, and the presence of occupied 5d$\pi$ MOs at lower energies are the salient electronic structural features. The occupied MOs of Pt(pop) lie 0.1−0.25 eV closer to the HOMO than in Pt(pop-$BF_2$). All the corresponding MOs have virtually the same compositions.

SO-TDDFT calculations of Pt(pop-$BF_2$) and Pt(pop) account for electronic absorption spectra across the entire UV−vis region, whereas spin-free TDDFT fails in the UV. Because of the large LUMO/LUMO+1 separation, all spectroscopically important transitions involve excitation into

**Table 6. Comparison of Low-Lying SO States of Pt(pop-$BF_2$) at the Ground-State, Lowest Singlet, and Lowest Triplet Geometries**

| SO state | contributions of spin−free states | character | energy ($cm^{-1}$) | $\Delta E^a$ ($cm^{-1}$) | $\lambda$ (nm) | oscillator strength |
|---|---|---|---|---|---|---|
| | | $a^1A_g$ ground-state geometry | | | | |
| $aA_u$ ($aA_{1u}$) | $a^3A_u$ (98%) + $c^3B_u$ (0.8%) + $d^3B_u$ (0.9%) + $b^3B_u$ (0.3%) | d$\sigma$*→p$\sigma$ | 20 278 | 0 | 493 | 0 |
| $aB_u$ ($aE_u$) | $a^3A_u$ (98%) + $d^1B_u$ (0.7%) + $c^3B_u$ (0.9%) + $b^3B_u$ (0.3%) | d$\sigma$*→p$\sigma$ | 20 332 | 54 | 493 | 0.000 26 |
| $bB_u$ ($aE_u$) | $a^3A_u$ (98%) + $f^1B_u$ (0.5%) + $a^1B_u$ (0.2%) + $b^3B_u$ (0.9%) | d$\sigma$*→p$\sigma$ | 20 338 | 60 | 492 | 0.000 17 |
| $bA_u$ ($aA_{2u}$) | $a^1A_u$ (95.6%) + $c^3B_u$ (1.4%) + $d^3B_u$ (1.4%) + $a^3B_u$ (0.9%) + $b^3B_u$ (0.6%) | d$\sigma$*→p$\sigma$ | 27 244 | 6966 | 367 | 0.230 |
| $cA_u$ | $a^3B_u$ (50%) + $b^3B_u$ (50%) | LMMCT p$\pi$→p$\sigma$ | 33 076 | 12 798 | 302 | 0.000 |
| $dA_u$ | $a^3B_u$ (50%) + $b^3B_u$ (50%) | LMMCT p$\pi$→p$\sigma$ | 33 076 | 12 798 | 302 | 0.000 |
| | | $a^1A_u$ geometry | | | | |
| $aA_u$ ($aA_{1u}$) | $a^3A_u$ (98%) + $c^3B_u$ (0.7%) + $d^3B_u$ (0.5%) + $b^3B_u$ (0.3%) | d$\sigma$*→p$\sigma$ | 18 220 | 0 | 549 | 0 |
| $aB_u$ ($aE_u$) | $a^3A_u$ (98.5%) + $d^1B_u$ (0.5%) + $c^3B_u$ (0.6%) + $b^3B_u$ (0.2%) | d$\sigma$*→p$\sigma$ | 18 272 | 52 | 547 | 0.000 07 |
| $bB_u$ ($aE_u$) | $a^3A_u$ (98.5%) + $f^1B_u$ (0.4%) + $a^1B_u$ (0.2%) + $b^3B_u$ (0.6%) | d$\sigma$*→p$\sigma$ | 18 285 | 65 | 547 | 0.000 04 |
| $bA_u$ ($aA_{2u}$) | $a^1A_u$ (97%) + $c^3B_u$ (0.7%) + $d^3B_u$ (0.9%) + $a^3B_u$ (0.5%) + $b^3B_u$ (0.4%) | d$\sigma$*→p$\sigma$ | 25 252 | 7032 | 396 | 0.218 |
| $cA_u$ | $a^3B_u$ (78%) + $b^3B_u$ (22%) | LMMCT p$\pi$→p$\sigma$ | 30 921 | 12 701 | 323 | 0.000 |
| $dA_u$ | $a^3B_u$ (79%) + $b^3B_u$ (21%) | LMMCT p$\pi$→p$\sigma$ | 30 956 | 12 736 | 323 | 0.000 |
| | | $a^3A_u$ geometry | | | | |
| $aA_u$ ($aA_{1u}$) | $a^3A_u$ (98%) + $c^3B_u$ (0.8%) + $d^3B_u$ (0.5%) + $b^3B_u$ (0.3%) | d$\sigma$*→p$\sigma$ | 18 144 | 0 | 551 | 0 |
| $aB_u$ ($aE_u$) | $a^3A_u$ (98.5%) + $d^1B_u$ (0.5%) + $c^3B_u$ (0.6%) + $b^3B_u$ (0.2%) | d$\sigma$*→p$\sigma$ | 18 209 | 52 | 549 | 0.000 04 |
| $bB_u$ ($aE_u$) | $a^3A_u$ (98.5%) + $f^1B_u$ (0.3%) + $a^1B_u$ (0.2%) + $b^3B_u$ (0.6%) | d$\sigma$*→p$\sigma$ | 18 216 | 65 | 549 | 0.000 06 |
| $bA_u$ ($aA_{2u}$) | $a^1A_u$ (97%) + $c^3B_u$ (0.7%) + $d^3B_u$ (0.9%) + $a^3B_u$ (0.5%) + $b^3B_u$ (0.4%) | d$\sigma$*→p$\sigma$ | 25 197 | 7053 | 397 | 0.218 |
| $cA_u$ | $a^3B_u$ (78%) + $b^3B_u$ (22%) | LMMCT p$\pi$→p$\sigma$ | 30 903 | 12 759 | 324 | 0.000 |
| $dA_u$ | $a^3B_u$ (79%) + $b^3B_u$ (21%) | LMMCT p$\pi$→p$\sigma$ | 30 941 | 12 759 | 323 | 0.000 |

[a] $\Delta E$ is the energy difference from the lowest SO excited state. Symmetry labeling corresponds to idealized $C_{2h}$ symmetry. ($D_{4h}$ labels in parentheses.) Calculation: SO TDDFT (COSMO-MeCN).



DOI: 10.1021/acs.inorgchem.5b00063
Inorg. Chem. 2015, 54, 3491−3500

the pσ LUMO, strengthening the Pt−Pt bond. The lowest two spin-free states ($a^3A_u$ and $a^1A_u$) have dσ*pσ character, with a dσ* → pop MLCT contribution that arises from LUMO delocalization over the ligands. SO interaction with high-lying dπpσ/LMMCT singlets ($d,f^1B_u$), and, to a lesser extent, LMMCT/pπpσ ($a^1B_u$) splits $a^3A_u$ to $aA_u$, $aB_u$, and $bB_u$ SO states. Transitions to $a,bB_u$ acquire nonzero oscillator strengths, allowing for weak absorption at 454 nm (and phosphorescence). The $a^1A_u$-based SO state $bA_u$ gives rise to the most prominent absorption band at ∼365 nm. It contains small admixtures of higher dπpσ triplets ($c,d^3B_u$), and, to a lesser extent, LMMCT/pπpσ $a,b^3B_u$ states that affect the photophysical properties. Interestingly, dσ*pσ-based states are SO-coupled only with states that contain excitations involving 5dπ or 6pπ orbitals that are orthogonal to the Pt−Pt ($z$) axis and, hence, to $d_{z2}σ^*$ and $p_zσ$ orbitals. Qualitatively, this symmetry restriction underscores the angular momentum rotation necessary for efficient SO coupling. SO coupling with dπpσ-based states is stronger than with LMMCT/pπpσ ones, despite a larger energy gap, likely attributable to the much larger Pt-localization of 5dπ-containing MOs (Supporting Information, Table S2).

The strong transition to $bA_u$ is followed by a series of weak UV transitions to states of predominantly triplet LMMCT character (with a small pπpσ admixture) that gain intensity through SO coupling (introducing 10−20% singlet character). Their excitation will strengthen the Pt−Pt interaction and reorganize the electron density over the ligand cluster. At the high-energy end of the UV spectrum are two transitions to states of mixed dπpσ*/LMMCT character ($h,jB_u$) that have higher intensity owing to 60−80% singlet character, at least for Pt(pop-$BF_2$). No transitions into SO states with significant contributions from excitations into σ*(Pt−P)/δ,δ*(Pt−Pt) orbitals contribute to the spectrum as their intensities are too low. The calculated gap between $bA_u$ and the closely spaced LMMCT manifold is larger for Pt(pop-$BF_2$) (5832 $cm^{-1}$) than for Pt(pop) (4197 $cm^{-1}$). Both calculated and experimental LMMCT and dπpσ/LMMCT transition energies increase upon changing Pt(pop) to Pt(pop-$BF_2$), presumably due to the stabilizing effect of electron-withdrawing $BF_2$ groups on occupied ligand-localized MOs.

The rate and mechanism of $a^1A_u \rightarrow {}^3A_u$ ($^1dσ^*pσ \rightarrow {}^3dσ^*pσ$) intersystem crossing (ISC) are the most intriguing aspects of Pt(pop-$BF_2$) photophysics. The $a^1A_u$ state is strongly fluorescent, decaying with a temperature-dependent lifetime (1.6 ns at 293 K in MeCN). The nonradiative ISC rate constant is $4.7 \times 10^8$ $s^{-1}$ (212 ns) at 293 K, with an activation energy of ∼2230 $cm^{-1}$.[1] In contrast, the $a^1A_u$ state of Pt(pop) decays much faster, with an ∼3 ps lifetime in MeCN and an activation barrier of 1190 $cm^{-1}$ in 2-Me-tetrahydrofuran/propionitrile.[14] The $1 \times 10^3$ to $1 \times 10^4$-fold difference in ISC rates between the two very similar complexes and the nature of the thermally activated pathway are two key unanswered questions in $d^8$−$d^8$ photophysics.

Our present calculations show that the optically populated $bA_u$ state and the lowest $aA_u$, $a,bB_u$ manifold are energetically isolated from each other as well as from higher excited states, both in ground-state and $a^1A_u$ (Pt−Pt contracted) geometries. They also confirm that the optimized structures of the $a^1A_u$ and $a^3A_u$ spin-free states (which are the predominant contributors to $bA_u$ and $aA_u/aB_u/bB_u$, respectively) are very similar, indicating nested potential energy surfaces. This finding accords with the observed equally spaced vibrational structure of $aA_g(GS) \rightarrow aB_u/bB_u$ and $aA_g(GS) \rightarrow bA_u$ absorption bands,[5−7] Pt(pop-$BF_2$) fluorescence and phosphorescence excitation bands,[16] and long-lived coherent oscillations of the Pt(pop) $bA_u$ state[4] that suggest harmonic potentials without low-lying crossings to other electronic states.

Direct SO interaction between spin-free "parent states" $a^1A_u$ and $a^3A_u$ is formally symmetry-allowed in $C_{2h}$ as well as $C_{4h}$ symmetries ($A_u⊗A_u = A_g(R_z)$). However, SO-TDDFT calculations do not show $a^1A_u$−$a^3A_u$ mixing, because rotation along the $z$(Pt−Pt) molecular axis cannot change the angular momentum of the $d_{z2}σ^*p_zσ$ state, which would be required to compensate for the spin-momentum change. Instead of direct SO coupling, the $a^1A_u \rightarrow a^3A_u$ ISC could occur through second-order interactions with $c,d^3B_u$(dπpσ) and $b^3B_u$(LMMCT/pπpσ) states that mix with both $a^3A_u$ and $a^1A_u$ in the SO states $aA_u/aB_u/bB_u$ and $bA_u$, respectively (Tables 3 and 4, Figure 4). Such SO interactions are fully allowed both in $C_{2h}$ ($A_u⊗B_u = B_g(R_x,R_y)$) and $D_{4h}$ core symmetries ($A_{2u}⊗E_u = E_g(R_x,R_y)$).

In terms of SO states, the ISC can be viewed as a nonradiative $bA_u \rightarrow aA_u/aB_u/bB_u$ transition (Figure 5). Within the perturbative approximation used herein, the ISC electronic coupling term contains vibronic integrals between the same-spin spin-free components of SO states, multiplied by corresponding mixing coefficients. All these terms will contain terms of the type $\langle {}^3A_u|\partial H/\partial Q_i|{}^3B_u\rangle^2/\Delta E$ and $\langle {}^1A_u|\partial H/\partial Q_i|{}^1B_u\rangle^2/\Delta E$, where $Q_i$ is the promoting vibration that must be $B_g$, if the vibronic integrals are to be nonzero. The overall coupling strength is small because $\Delta E$, the energetic separation of the dσ*pσ states from higher-lying interacting states, is very large. These arguments are applicable only to weak coupling between $a^1A_u$ and $b^3A_u$ potential energy surfaces, close to $a^1A_u$ minimum (Figure 6). They do not account for the vastly different ISC rates between Pt(pop-$BF_2$) and Pt(pop), although additional admixture of higher dπpσ/LMMCT singlets $e,f^1B_u$ to both $bA_u$ *and* $a,bB_u$ states in Pt(pop) (Table 5) could open another second-order SO mixing pathway, and the slightly

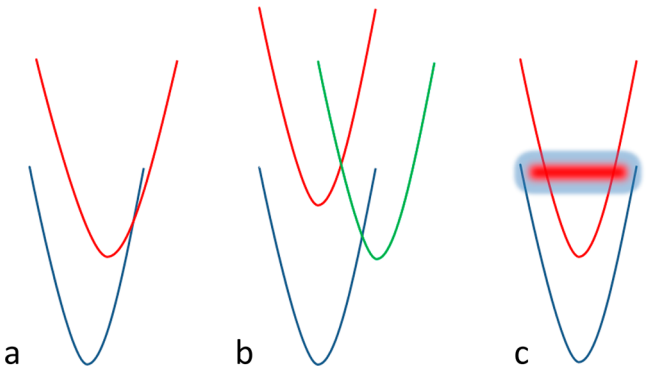


**Figure 6.** Alternative ISC mechanisms in [Pt(pop)] and [Pt(pop-$BF_2$)]. (a) Crossing between the singlet (red) and triplet (blue) excited states along an asymmetric coordinate that is not coupled to spectroscopic transitions to/from the ground state. Present calculations did not reveal any coordinate along which the $^1A_{2u}$ and $^3A_{2u}$ structures are sufficiently different. However, this situation could possibly occur along large-amplitude, low-frequency skeletal distortions or upon solvent and/or counter-cation fluctuations. (b) ISC via an intermediate state (green). (c) A "resonance" region (shaded area) of strong electronic interaction and/or FC overlap is assumed to occur upon excitation of large-amplitude, low-frequency skeletal or solvent asymmetric modes.



DOI: 10.1021/acs.inorgchem.5b00063
*Inorg. Chem.* 2015, 54, 3491−3500

larger difference between the Pt−Pt bond lengths in $a^1A_u$ and $b^3A_u$ states could increase the Franck−Condon factor.

The temperature-dependent ISC pathway is attributable either to direct crossing between $bA_u$ and $aA_u/aB_u/bB_u$ potential energy surfaces above the $bA_u$ minimum (Figure 6a) or to transient population of an intermediate state (Figure 6b). Direct crossing is unlikely because the states involved have virtually identical structures. The putative intermediate state would have to be strongly coupled both to the initial $bA_u$ state and to at least one of the final states $aA_u/aB_u/bB_u$. In terms of spin-free states, this condition requires the intermediate state to be either $^1B_u$ (vibronicaly coupled to $a^1A_u$, SO-coupled to $^3A_u$) or $^3B_u$ (SO coupled to $a^1A_u$, vibronically to $a^3A_u$). Moreover, such a state would have significant contributions from excitations involving Pt 5d$\pi$ and/or 6p$\pi$ orbitals. Several such states ($a,b,d,f^1B_u$; $a,b,c,d^3B_u$) are identified in Table 3 (Supporting Information, Table S4 for Pt(pop)), but their energies are much higher ($\geq$5900 and $\geq$15 650 $cm^{-1}$ for LMMCT/p$\pi$p$\sigma$ and d$\pi$p$\sigma$, respectively) above $a^1A_u$ than the experimental activation energy (2230 $cm^{-1}$). The same energetic mismatch is obtained in the SO framework, where the lowest LMMCT/p$\pi$p$\sigma$ SO state was calculated 5832 $cm^{-1}$ above $bA_u$ in the ground-state geometry (4197 $cm^{-1}$ for Pt(pop)). These energy gaps are only slightly smaller in the more relevant $a^1A_u$ geometry with the contracted Pt−Pt bond: 5669 and 3814 $cm^{-1}$, respectively (Table 6 and Supporting Information, Table S5). It could be possible, however, that the activated ISC pathway follows a different coordinate, one in which the intermediate state drops in energy and becomes thermally accessible. In this respect, we can also reiterate our previous suggestion[1] that structural fluctuations transiently distort the $Pt_2P_8$ core to a configuration with sufficient $a^1A_u$ − $a^3A_u$ SO coupling, allowing for direct ISC without surface crossing and without invoking upper states (Figure 6c). Structural flexibility of Pt(pop) would facilitate such transient distortions, accounting for much faster ISC as compared with rigid Pt(pop-$BF_2$).

## CONCLUSIONS

We emphasize that inclusion of SO coupling is essential if we are to understand the spectroscopy and photophysics of $d^8$−$d^8$ diplatinum complexes. Perturbational SO TDDFT is a tractable approach leading to results that are in good agreement with experiment, provided that a sufficiently large number of states above the lowest excited state is included in the calculation. Spin−orbit TDDFT calculations emerge[25,32−34] as a promising technique to shed light on ISC mechanisms in transition metal complexes.

The electronic structures of Pt(pop) and Pt(pop-$BF_2$) can be understood in terms of energetically isolated d$\sigma$*p$\sigma$ excited states along with a higher-lying manifold of LMMCT states, some with PtPt p$\pi$p$\sigma$ and d$\pi$p$\sigma$ contributions. The d$\sigma$*p$\sigma$ states largely retain singlet and triplet character, whereas extensive spin-mixing occurs in LMMCT states, thereby accounting for several absorption features in the UV region. The lowest d$\sigma$*p$\sigma$ triplet is split into three SO states through interactions with high-lying LMMCT d$\pi$p$\sigma$ and p$\pi$p$\sigma$ singlets. Notably, second-order SO coupling between the d$\sigma$*p$\sigma$ singlet and triplet via mixing with high-lying $^3$d$\pi$p$\sigma$/LMMCT and (to a lesser extent) $^3$LMMCT/p$\pi$p$\sigma$ states affects photophysical behavior, and additional coupling through $^1$d$\pi$p$\sigma$/LMMCT possibly contributes in the case of Pt(pop). One contributor to the dramatically different intersystem crossing rates of the two complexes could be the greater structural flexibility of Pt(pop), thereby lowering the barriers to configurations that are more strongly SO-coupled.

## ASSOCIATED CONTENT

### Supporting Information

Selected experimental and calculated bond lengths, energies and compositions of molecular orbitals of Pt(pop-$BF_2$) and Pt(pop), calculated spin-free electronic transitions of Pt(pop), and SO states of Pt(pop) at ground- and excited-state geometries. Illustrated DFT-optimized structures, X-ray crystallographic data. This material is available free of charge via the Internet at http://pubs.acs.org.

## AUTHOR INFORMATION

### Corresponding Authors

*E-mail: zalis@jh-inst.cas.cz. (S.Z.)
*E-mail: hbgray@caltech.edu. (H.B.G.)
*E-mail: a.vlcek@qmul.ac.uk. (A.V.)

### Notes

The authors declare no competing financial interest.

## ACKNOWLEDGMENTS

We thank Mr. L. Henling (Beckman Institute) for his help with determining and presenting the X-ray structure. This work was supported by the Ministry of Education of the Czech Republic Grant No. LH13015 (Program KONTAKT II), the NSF CCI Solar Fuels Program (CHE-1305124), and the Arnold and Mabel Beckman Foundation.

## REFERENCES

(1) Durrell, A. C.; Keller, G. E.; Lam, Y.-C.; Sýkora, J.; Vlček, A., Jr.; Gray, H. B. *J. Am. Chem. Soc.* **2012**, *134*, 14201−14207.
(2) Che, C.-M.; Butler, L. G.; Gray, H. B.; Crooks, R. M.; Woodruff, W. H. *J. Am. Chem. Soc.* **1983**, *105*, 5492−5494.
(3) van der Veen, R. M.; Milne, C. J.; El Nahhas, A.; Lima, F. A.; Pham, V.-T.; Best, J.; Weinstein, J. A.; Borca, C. N.; Abela, R.; Bressler, C.; Chergui, M. *Angew. Chem., Int. Ed.* **2009**, *48*, 2711−2714.
(4) van der Veen, R. M.; Cannizzo, A.; van Mourik, F.; Vlček, A., Jr.; Chergui, M. *J. Am. Chem. Soc.* **2011**, *133*, 305−315.
(5) Rice, S. F.; Gray, H. B. *J. Am. Chem. Soc.* **1983**, *105*, 4571−4575.
(6) Fordyce, W. A.; Brummer, J. G.; Crosby, G. A. *J. Am. Chem. Soc.* **1981**, *103*, 7061−7064.
(7) Stiegman, A. E.; Rice, S. F.; Gray, H. B.; Miskowski, V. M. *Inorg. Chem.* **1987**, *26*, 1112−1116.
(8) Peterson, J. R.; Kalyanasundaram, K. *J. Phys. Chem.* **1985**, *89*, 2486−2492.
(9) Sweeney, R. J.; Harvey, E. L.; Gray, H. B. *Coord. Chem. Rev.* **1990**, *105*, 23−34.
(10) Roundhill, D. M.; Gray, H. B.; Che, C.-M. *Acc. Chem. Res.* **1989**, *22*, 55−61.
(11) Smith, D. C.; Gray, H. B. In *The Challenge of d and f Electrons;* Salahub, D. R., Zerner, M. C., Eds.; ACS Symposium Series 394; American Chemical Society: Washington, DC, 1989; pp 356−365.
(12) Vlček, A., Jr.; Gray, H. B. *J. Am. Chem. Soc.* **1987**, *109*, 286−287.
(13) Vlček, A., Jr.; Gray, H. B. *Inorg. Chem.* **1987**, *26*, 1997−2001.
(14) Milder, S. J.; Brunschwig, B. S. *J. Phys. Chem.* **1992**, *96*, 2189−2196.
(15) Markert, J. T.; Clements, D. P.; Corson, M. R.; Nagle, J. K. *Chem. Phys. Lett.* **1983**, *97*, 175−179.
(16) Hofbeck, T.; Lam, Y. C.; Kalbáč, M.; Záliš, S.; Winkler, J. R.; Yersin, H.; Vlček, A., Jr.; Gray, H. B. *manuscript in preparation.*
(17) Shimizu, Y.; Tanaka, Y.; Azumi, T. *J. Phys. Chem.* **1984**, *88*, 2423−2425.


DOI: 10.1021/acs.inorgchem.5b00063
*Inorg. Chem.* 2015, 54, 3491−3500

(18) Gellene, G. I.; Roundhill, D. M. *J. Phys. Chem. A* **2002**, *106*, 7617−7620.
(19) Novozhilova; Volkov, A. V.; Coppens, P. *J. Am. Chem. Soc.* **2003**, *125*, 1079−1087.
(20) Stoyanov, S. R.; Villegas, J. M.; Rillema, D. P. *J. Phys. Chem. B* **2004**, *108*, 12175−12180.
(21) Pan, Q.-J.; Fu, H.-G.; Yu, H.-T.; Zhang, H.-X. *Inorg. Chem.* **2006**, *45*, 8729−8735.
(22) Wang, F.; Ziegler, T. *J. Chem. Phys.* **2005**, *123*, 154102.
(23) Wang, F.; Ziegler, T.; van Lenthe, E.; van Gisbergen, S.; Baerends, E. J. *J. Chem. Phys.* **2005**, *122*, 204103.
(24) Li, Z.; Suo, B.; Zhang, Y.; Xiao, Y.; Liu, W. *Mol. Phys.* **2013**, *111*, 3741−3755.
(25) Baková, R.; Chergui, M.; Daniel, C.; Vlček, A., Jr.; Záliš, S. *Coord. Chem. Rev.* **2011**, *255*, 975−989.
(26) Te Velde, G.; Bickelhaupt, F. M.; van Gisbergen, S. J. A.; Fonseca Guerra, C.; Baerends, E. J.; Snijders, J. G.; Ziegler, T. *J. Comput. Chem.* **2001**, *22*, 931−967.
(27) *ADF2013.01, SCM, Theoretical Chemistry;* Vrije Universiteit: Amsterdam, The Netherlands; http://www.scm.com.
(28) Perdew, J. P.; Burke, K.; Ernzerhof, M. *Phys. Rev. Lett.* **1996**, *77*, 3865−3868.
(29) Adamo, C.; Barone, V. *J. Chem. Phys.* **1999**, *110*, 6158−6170.
(30) Klamt, A.; Schüürmann, G. *J. Chem. Soc., Perkin Trans. 2* **1993**, 799−805.
(31) Che, C.-M.; Butler, L. G.; Grunthaner, P. J.; Gray, H. B. *Inorg. Chem.* **1985**, *24*, 4662−4665.
(32) Heydová, R.; Gindensperger, E.; Romano, R.; Sýkora, J.; Vlček, A., Jr.; Záliš, S.; Daniel, C. *J. Phys. Chem. A* **2012**, *116*, 11319−11329.
(33) Sousa, C.; de Graaf, C.; Rudavskyi, A.; Broer, R.; Tatchen, J.; Etinski, M.; Marian, C. M. *Chem.—Eur. J.* **2013**, *19*, 17541−17551.
(34) Gourlaouen, C.; Daniel, C. *Dalton Trans.* **2014**, *43*, 17806−17819.



DOI: 10.1021/acs.inorgchem.5b00063
*Inorg. Chem.* 2015, 54, 3491−3500